Controlling the interactions of space-variant polarization beams with rubidium vapor using external magnetic fields

Liron Stern,[1,2] Anat Szapiro,[1,2] Eliran Talker,[1] and Uriel Levy[1,*]

[1]*Department of Applied Physics, The Benin School of Engineering and Computer Science, The Hebrew University of Jerusalem, Jerusalem, 91904, Israel*

[2]*Contributed equally*

[*]*ulevy@mail.huji.ac.il*

Abstract: Space variant beams are of great importance for a variety of applications that have emerged in recent years. As such, manipulation of their degrees of freedom is highly desired. Here, we study the general interaction of space variant beams with a magnetically influenced Rb medium exploiting the atoms versatile properties in terms of frequency and intensity dependent circular dichroism and circular birefringence. We present the particular cases of radially polarized and hybrid polarized beams where the control of the polarization states is demonstrated experimentally. Moreover, we show that such an atomic system can be used as a tunable analyzer for space variant beams. Finally, exploiting the non-linear properties of Rb vapor, we show that we can control the circular birefringence all optically, and thus modulate the polarization of the radial polarized beam.

OCIS codes: (260.5430) Polarization; (160.3820) Magneto-optical materials; (260.7490) Zeeman effect; (300.6210) Spectroscopy, atomic.

References and links

1. G. M. Lerman and U. Levy, "Effect of radial polarization and apodization on spot size under tight focusing conditions," Opt. Express **16**(7), 4567–4581 (2008).
2. R. Dorn, S. Quabis, and G. Leuchs, "Sharper focus for a radially polarized light beam," Phys. Rev. Lett. **91**(23), 233901 (2003).
3. Q. Zhan, "Cylindrical vector beams: from mathematical concepts to applications," Adv. Opt. Photon., AOP **1**, 1–57 (2009).
4. G. M. Lerman, A. Yanai, N. Ben-Yosef, and U. Levy, "Demonstration of an elliptical plasmonic lens illuminated with radially-like polarized field," Opt. Express **18**(10), 10871–10877 (2010).
5. P. R. Dolan, X. Li, J. Storteboom, and M. Gu, "Complete determination of the orientation of NV centers with radially polarized beams," Opt. Express **22**(4), 4379–4387 (2014).
6. I. Nishiyama, N. Yoshida, Y. Otani, and N. Umeda, "Single-shot birefringence measurement using radial polarizer fabricated by direct atomic force microscope stroking method," Meas. Sci. Technol. **18**(6), 1673–1677 (2007).
7. O. Firstenberg, P. London, M. Shuker, A. Ron, and N. Davidson, "Elimination, reversal and directional bias of optical diffraction," Nat. Phys. **5**(9), 665–668 (2009).
8. F. K. Fatemi, "Cylindrical vector beams for rapid polarization-dependent measurements in atomic systems," Opt. Express **19**(25), 25143–25150 (2011).
9. L. Weller, K. S. Kleinbach, M. A. Zentile, S. Knappe, I. G. Hughes, and C. S. Adams, "Optical isolator using an atomic vapor in the hyperfine Paschen-Back regime," Opt. Lett. **37**(16), 3405–3407 (2012).
10. R. M. Camacho, M. V. Pack, and J. C. Howell, "Slow light with large fractional delays by spectral hole-burning in rubidium vapor," Phys. Rev. A **74**(3), 033801 (2006).
11. A. M. C. Dawes, L. Illing, S. M. Clark, and D. J. Gauthier, "All-Optical switching in rubidium vapor," Science **308**(5722), 672–674 (2005).
12. N. A. Proite, B. E. Unks, J. T. Green, and D. D. Yavuz, "Refractive index enhancement with vanishing absorption in an atomic vapor," Phys. Rev. Lett. **101**(14), 147401 (2008).
13. S. Knappe, P. Schwindt, V. Shah, L. Hollberg, J. Kitching, L. Liew, and J. Moreland, "A chip-scale atomic clock based on 87Rb with improved frequency stability," Opt. Express **13**(4), 1249–1253 (2005).

#256044 Received 18 Dec 2015; revised 13 Feb 2016; accepted 14 Feb 2016; published 25 Feb 2016

14. D. Budker and M. Romalis, "Optical magnetometry," Nat. Phys. **3**(4), 227–234 (2007).
15. M. Hosseini, B. M. Sparkes, G. Campbell, P. K. Lam, and B. C. Buchler, "High efficiency coherent optical memory with warm rubidium vapour," Nat. Commun. **2**, 174 (2011).
16. S. Krishnamurthy, Y. Wang, Y. Tu, S. Tseng, and M. S. Shahriar, "High-speed modulation in ladder transitions in Rb atoms using high-pressure buffer gas," Opt. Express **23**(9), 11470–11482 (2015).
17. P. Siddons, C. S. Adams, C. Ge, and I. G. Hughes, "Absolute absorption on rubidium D lines: comparison between theory and experiment," J. Phys. At. Mol. Opt. Phys. **41**(15), 155004 (2008).
18. B. Gu, Y. Pan, G. Rui, D. Xu, Q. Zhan, and Y. Cui, "Polarization evolution characteristics of focused hybridly polarized vector fields," Appl. Phys. B **117**(3), 915–926 (2014).
19. G. M. Lerman, L. Stern, and U. Levy, "Generation and tight focusing of hybridly polarized vector beams," Opt. Express **18**(26), 27650–27657 (2010).

1. Introduction

In recent years, the optical properties of space variant polarized beams, that is, beams that have several spatial inhomogeneous polarization states, have drawn significant attention. Such beams have been the topic of numerous theoretical and experimental investigations due to the variety of their potential applications, including tight focus and optical trapping [1–4], particle orientation analysis [5], and single shot polarization dependent measurements [6]. Utilizing the spatial degrees of freedom of light interacting with atomic vapor has already been demonstrated to supply a rich platform [7] for studying diffusive properties of vapor in the presence of buffer gases. More recently, the additional degree of freedom of polarization has been introduced, and the interaction of space variant polarized beams and atoms has been explored [8].

Atomic systems, such as Rubidium (Rb) and Cesium have already been demonstrated as excellent elements for studying a variety of fundamental light vapor phenomena. Such vapors are highly versatile, primarily due to the variety of ways of controlling their properties, e.g. by optical, RF, magnetic or electrostatic fields. As a result, it is possible to manipulate the major degrees of freedom of light, including its polarization [9], speed of propagation [10], amplitude [11], phase [12] as well as its spectral properties. Indeed, alkali vapors are used extensively both in industry and academia for a myriad of applications spanning from time keeping [13] and magnetometry [14] to optical memories [15] and high speed all optical modulation [16].

Here, we combine these two exciting fields and demonstrate light matter interactions between space-variant polarization beams and magnetically influenced Rb vapor. By combining a versatile element such as Rb with space variant beams, and taking advantage of its high Verdet constant [9], we can obtain a space variant frequency and intensity dependent dichroic and birefringent system. By doing so, we demonstrate the manipulation of the spatial intensity and polarization distribution across the vector beams. Additionally, we have used the Rb cell as an efficient probe for imaging the local state of polarization across the beam. Finally, exploiting the non-linear properties of Rb vapor, we were able to control the circular birefringence all optically, enabling polarization rotation on the radial polarized beam.

2. Concept and theoretical considerations

Our experimental apparatus is described schematically in Fig. 1(a). Here, we sketch a hybrid space variant beam interacting with Rb atomic vapor which is under the application of an external magnetic field in the Faraday configuration. In such case, the hyperfine levels degeneracy is removed, and each level is split into 2F + 1 (F being the total spin quantum number) levels (see the top of Fig. 1(a), describing schematically the F = 2 to F' = 2 level scheme. Here the blue lines represent σ + transition, and the gray represent σ- transitions). As a consequence, the splitting of these energy levels changes their absorption spectra. This, together with the predefined selection rules, makes the Rb medium highly dichroic and birefringent for right-hand and left hand circular polarization (RHC and LHC respectively). As a result, while propagating within the medium, the hybrid beam changes its state of polarization, as illustrated in Fig. 1(a).

#256044 Received 18 Dec 2015; revised 13 Feb 2016; accepted 14 Feb 2016; published 25 Feb 2016

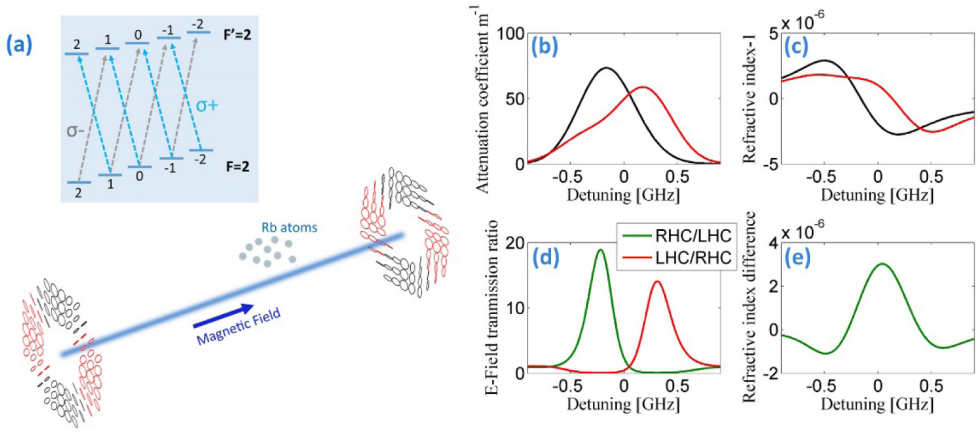

Fig. 1. (a) ^{85}Rb F = 2 to F' = 2 schematic level diagram and a sketch showing space-variant polarized beams interacting with Rb atoms in the presence of magnetic field. (b-e) Calculated frequency dependent (b) Attenuation coefficient and (c) Refractive index of Zeeman-shifted D1 F = 2 to F' = 2 and F' = 3 Doppler broadened transitions for RHC (red) and LHC (black) in a magnetic field of B = 180G. (d) the ratio between RHC and LHC (and the inverse ratio) electric field transmission (e) The difference between LHP and RHP refractive index.

To quantify this effect, we plot the numerical calculation of the attenuation coefficient, (Fig. 1(b)) and the refractive index (Fig. 1(c)) of ^{85}Rb D1 F = 2 to F' excited manifold Doppler broadened transitions under the influence of a magnetic field (B = 180 Gauss) in the linear regime. The choice of this specific transition throughout this work, is due to its relative spectral isolation in respect to ^{87}Rb lines, making it easier to interpret our results. The calculation is based on a slightly modified version of the procedure described in [17], which allows to find the atomic susceptibility in the presence of the linear Zeeman shift. As previously discussed, the application of the magnetic field removes the degeneracy. As a result, a different frequency response in both the attenuation coefficient and refractive index is obtained under RHP (red) and LHP (black) excitation. Next, to further quantify this numerical result we plot in Fig. 1(d) the ratio between the electric field transmission coefficient for RHC and LHC. For the sake of ease of comparison we also plot the opposite ratio, namely LHC to RHC. Clearly, we have obtained a circular dichroic (CD) frequency-dependent media. The calculation is performed using a propagation length of 7.5 cm, and atomic density of $2.5\cdot10^{11}$cm^{-3}. This circular dichroism reaches a ratio of 18.9 for a detuning of –210 MHz in favor of RHC, and 13.9 for a detuning of 330 Mhz in favor of LHC. Around zero detuning, this ratio is an order of magnitude smaller. Clearly, we have an asymmetry in the circular dichroism with respect to the zero detuning point, which is a direct consequence of the existence of two absorption lines (F = 2 to F' = 2 and F' = 3). Although the splitting of each individual line possess a mirror symmetry, the combination of the splitting and offset of these two lines violates the overall mirror symmetry. Following, in Fig. 1(e) we plot the difference in the refractive index between RHP and LHP as a function of frequency, where this difference creates a circularly birefringent (CB) frequency-dependent media. For the above mentioned atomic density and magnetic field, the refractive index difference reaches the value of $3\cdot10^{-6}$ corresponding to a polarization rotation of about 50°. For the calculation, we have used the linear Zeeman regime approximation for which the shift in the energy levels is given by $\Delta E \approx \mu_B g_F B$, where μ_B is the Bohr magneton, is g_F the Lande g-factor and B is the applied magnetic field. We note that this approximation is valid as long as the Zeeman shift is smaller than the hyperfine energy structure. In the experimental work presented here, the excited states ($5^2P_{3/2}$) exceed the linear approximation regime for several of the applied magnetic field values. Nevertheless, the physical mechanism remains the same. Obviously, in the

#256044 Received 18 Dec 2015; revised 13 Feb 2016; accepted 14 Feb 2016; published 25 Feb 2016

absence of magnetic field, the RHP and LHP extinction coefficient and refractive index coincides. As evident from Fig. 1, dichroism and birefringence are achieved by the application of a magnetic field. These two phenomena have strong yet different frequency dependency. For example, in the regime of zero frequency detuning (defined as the unperturbed resonance position) dichroism is barely observed (zero change in the absorption coefficient). Nevertheless, in the same frequency detuning region the difference in refractive index between RHP and LHP is maximal, resulting a media with large CB. A small change in the detuned frequency (~0.25 GHz) will drastically change this scenario by creating a different ratio between the CD and CB. It is this strong frequency-dependency which allows us to manipulate the amount of CB and CD in the medium.

Next, we describe the interaction of space-variant polarization with such CD and CB media. A general field of space-variant angular dependent polarized light can be written in a circularly polarized base as $E(\theta) = g(\theta)\hat{\sigma}_+ + f(\theta)\hat{\sigma}_-$, where g and f are complex functions in the angular polar coordinate θ, and $\hat{\sigma}_+$, $\hat{\sigma}_-$ are the Jones vectors of RHP and LHP. In this work we focus on two types of space-variant polarization beams: The first is the radially polarized beam, which is a beam of light with linear polarization directed towards the center of the beam. In general, the electric field of a radially polarized beam undergoing CB and CD can be described by:

$$E(\theta,\phi,a) \sim [ae^{i(\theta+\phi)}\hat{\sigma}_+ + e^{-i\theta}\hat{\sigma}_-], \quad (1)$$

where a represents the CD – the relative ratio in absorption between RHC and LHC, and φ represents the induced phase difference between these two polarizations, which causes CB to occur. The second type of beam we investigate is the more general hybrid polarization beam (HPB). Such a beam consists of spatially separated linear, elliptical, right-hand and left-hand circular polarization. HPB can be expressed as:

$$E(\delta,\phi,a) \sim [ae^{i\phi}(e^{i\delta} - ie^{-i\delta})\hat{\sigma}_+ + (e^{i\delta} + ie^{-i\delta})\hat{\sigma}_-], \quad (2)$$

where a is the CD, θ represents the phase difference between RHC and LHC, $\delta = m\theta + 2\pi nr^2/r_0 + \theta_0$, where m is a nonnegative integer that represents the azimuthal index, the arbitrary number n is the radial index, r_0 is the radius of the vector field, θ_0 is the initial phase and r, θ are the spatial coordinates in a cylindrical coordinate system [18].

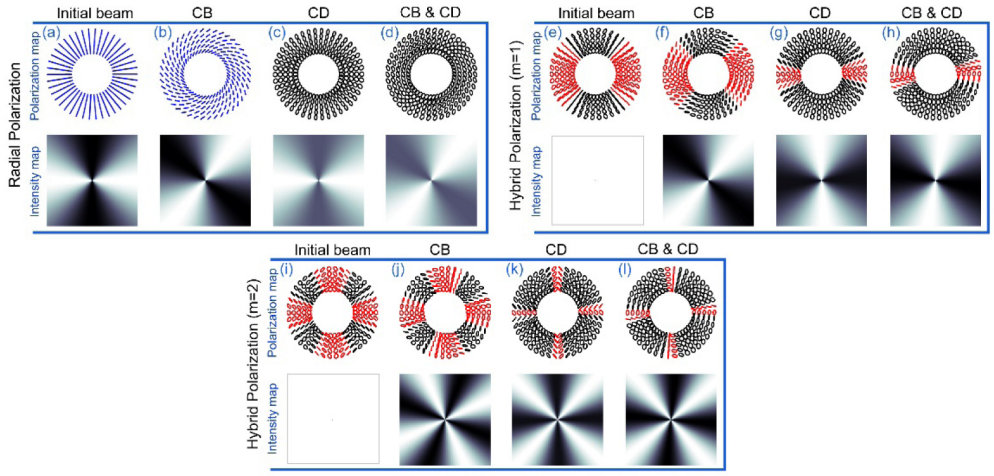

Fig. 2. Numerical calculations of the polarization and intensity distribution for three different space-variant beams after propagating through CB, CD and combined media. (a-d) radially polarized beam (e-h) hybrid polarized beam with m = 1, n = 0 and (i-l) hybrid polarized beam with m = 2, n = 0. The top panel of each type of beam represents the polarization distribution

#256044 Received 18 Dec 2015; revised 13 Feb 2016; accepted 14 Feb 2016; published 25 Feb 2016

while the intensity distribution (obtained by projecting the beam onto a horizontally aligned analyzer) is given in the bottom panel. The colors represent the polarization orientation - red and black correspond to RHP and LHP respectively and blue to linear polarization.

In order to describe the influence of a Zeeman-shifted Rb medium on space-variant beams we plot the polarization map and the intensity distribution (obtained by projecting the beam onto a horizontally aligned analyzer) of a radially polarized beam and two types of hybrid polarized beams propagating through CB medium, CD medium and a medium which combines both effects. In order to plot such polarization maps, we chose specific values of CD and CB, corresponding to a small detuning of –40 MHz. According to Fig. 1(d) and 1(e) such detuning corresponds to a CD transmission ratio of 4, and CB (in terms of polarization rotation) of about 45°. We use Eq. (1) and 2 to plot the polarization and intensity maps presented Fig. 2. Each of the mechanisms has a different role in affecting the properties of the beam. For instance, one can observe in columns b, f and j that the CB medium rotates the polarization direction homogenously in space while the beam maintains its polarization partitioning – i.e. the portions of its linear, circular and elliptical polarization remain unchanged. This is the opposite of the CD medium (column c, g and k), which maintains the polarization direction of the transmitted beam while changing its polarization partitioning (note the change in ratio between the black and the red areas). For example, Fig. 2(b) demonstrates the homogenous linear polarization rotation of the beam transmitted through the CB medium, whereas Fig. 2(c) shows the polarization transition from linear to elliptical produced by the CD medium. Here, the orientation of both principal axes of the elliptical polarization remains unchanged with respect to the original beam. Clearly, the influence of both CD and CB media is a combination of the two effects as can be seen in columns d, h and l. Note that the intensity maps in Fig. 2(e) and 2(k) are uniform, as the projection on the analyzer is constant.

3. Results

We now turn to describe the experimental apparatus, which is illustrated in Fig. 3(a). A DFB Diode Laser (Toptica DL100 beam diameter of 2mm) was scanned around the Rb D1 manifold. We used a radial polarization converter (RPC, Altechna) to create the radially polarized beams; the generation of a hybrid polarization beam with $m = 1$ and $n = 0$ was established by propagating the radially polarized beam through a quarter wave plate (QWP) [19]. To measure the polarization states of the space variant polarization beam, we characterized its Stokes parameters by taking four independent measurements using a QWP, a linear polarizer (analyzer) and a CCD camera. An external magnetic field was induced by applying current through a copper solenoid to create a magnetic field of about 180 G (measured by a Gauss meter). To increase the Rb density, the 7.5 cm long cell was heated to around 70°C. The power levels of the laser were attenuated in order to avoid saturation of the Rb transitions.

First, we demonstrate the radial Faraday Effect, i.e. the effect described by Fig. 2(a) panel 2. To do so, we detune the laser to a spectral regime where CB is dominant over CD. In the top panel of Fig. 3(b) we plot the intensity distribution as captured by the camera in the presence of a horizontally aligned analyzer, with (left) and without (right) applying a magnetic field. A nearly 45° polarization rotation is observed (estimated both from the stokes measurements, and the intensity distribution). The obtained spatial polarization distribution can be helpful in identifying the polarization rotation in single shot measurement. Otherwise, one needs at least two sequential measurements. Here, the polarization rotation angle can be simply extracted from the orientation of the rotated symmetry axis of the beam intensity (Fig. 3(b), top). This is a unique property of the space variant polarized beam. Next, we conduct a Stokes parameters characterization in the presence and the absence of the magnetic field, and plot the respective polarization map in Fig. 3(b) (bottom panel). We use a grid of approximately 20 points, with a distance between each grid point of ~0.1mm. Each point is

#256044 Received 18 Dec 2015; revised 13 Feb 2016; accepted 14 Feb 2016; published 25 Feb 2016

box-averaged using approximately 20X20 pixels. Clearly, one observers a polarization rotation of the radially polarized beam, similar to the simulated data presented in Fig. 2(b).

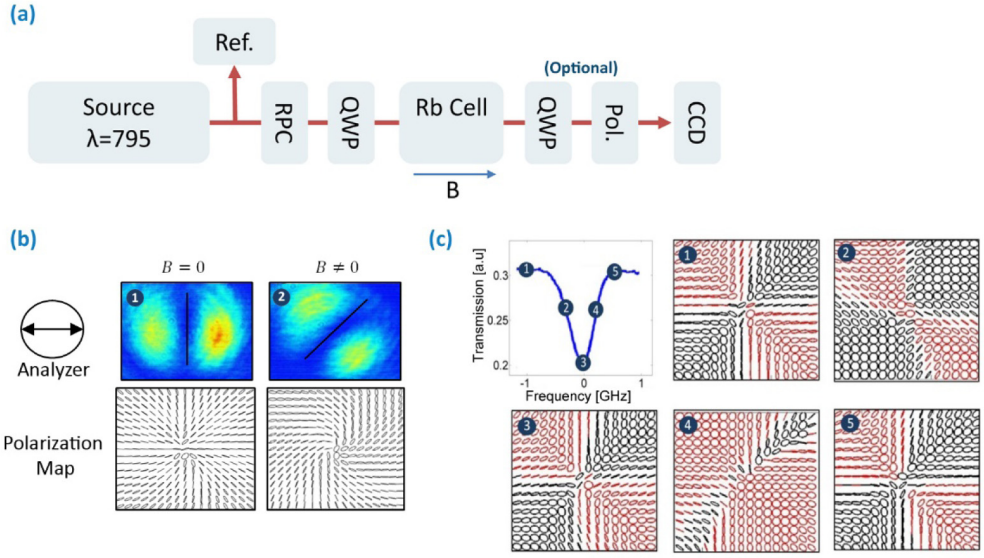

Fig. 3. (a) Schematic sketch of experimental arrangement (b) Single shot measurements of radially polarized beam intensity projected on a horizontally aligned analyzer (top) and polarization map (bottom) without (left) and with (right) the applied magnetic field (c) Measured polarization distribution obtained from full Stokes parameters of a HPB transmitted through the Rb medium at different wavelengths. Red is for RHP and black is for LHP. Top left shows the absorption spectrum of the reference cell and the measured points.

Next, we turn to characterize the interaction of a hybrid polarized beam with the Rb medium. In Fig. 3(c) we plot the measured polarizations distribution of the hybrid polarized beam (m = 1) after interacting with Rb in the near resonance D1 transition regime in the presence of magnetic field. Different wavelength regimes show different ratios between CD and CB in the media, as described below. Panels 1, 5 show practically no influence of either CD or CB on the transmitted beam, as expected in the off-resonance regime. Indeed, the initial beam polarization distribution of the transmitted beam before entering the magnetically influenced Rb medium (not shown) resembles almost exactly the polarization distribution shown in panels 1, 5. In contrast, panel 2 shows a CD effect; in this regime the RHP has a higher absorption coefficient and thus the major polarizations of the transmitted beam are LHP. This effect is even more dominant in panel 4, which presents a similar yet opposite picture with an opposite CD. The notable asymmetry between panels 2 and 4 are directly related to the asymmetry in the dichroism presented in Fig. 1(d), where for a detuning of 200MHz, the ratio between the transmission coefficients of RHC and LHC can differ by a factor of two. In panel 3 CB is noticeable (about 30° of polarization rotation compared to the off-resonance polarization distribution) while CD is barely observed. When comparing these polarization distributions to the calculated ones in Fig. 2, one can observe a qualitative resemblance. For instance, the case of a dominate CD in Fig. 3(c,4) resembles Fig. 2(g) (albeit rotated in 45 degrees, due to the initial orientation of the quarter wave plate in respect to the principal axis), and the case of dominate CB in Fig. 3(c,3) resembles Fig. 2(f). Some quantitative difference may be the result of an inhomogeneous magnetic field as well as deviation from the Zeeman approximation into the Paschen-Back regime.

#256044 Received 18 Dec 2015; revised 13 Feb 2016; accepted 14 Feb 2016; published 25 Feb 2016

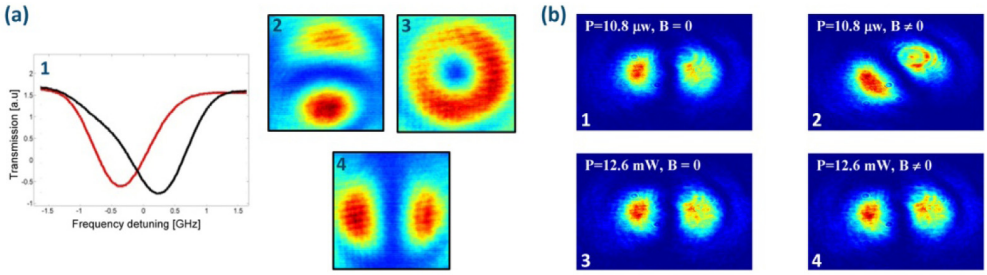

Fig. 4. (a,1) Measured transmission spectra of a magnetically controlled ^{85}Rb transition manifold for RHP and LHP (red and black, respectively). (a,2-4) measured transmission of the HPB at various wavelengths (a,2) in the regime of RHP resonance (a,3) in the regime of equivalent absorption between RHP and LHP (a,4) regime of LHP resonance. b) measured transmission of radialy polarized light in the regime of CB: (b,1) at low intensity and no magnetic field, (b,2) low intensity and magnetic field (b,3) at high intensity and no magnetic field, (b,4) high intensity and magnetic field.

Subsequently, we demonstrate the usefulness of our approach for the application of tunable space variant analyzer. First, we plot in Fig. 4(a,1) the measured absorption spectra for RHP and LHP polarization in the F = 2 to F' = 2 and F' = 3 ^{85}Rb transition. Next we plot measured transmission distribution for three frequencies in reference to Fig. 4(a,1). The first image (Fig. 4(a,2)) is captured at the frequency region of RHP resonance (approx.-0.3 GHz detuning from the unperturbed resonance). Here, the cross section area in the beam containing RHP is absorbed while the cross section area with LHP is transmitted and captured by the camera. Similarly, Fig. 4(a,4) show an image captured by tuning the laser frequency near the LHP resonance (+ 0.3GHz). In such a case, the cross section area in the beam with LHP is absorbed while the cross section area with RHP is transmitted and captured by the camera. Finally, when the absorption coefficients of RHP and LHP are equal (zero detuning, Fig. 4(a,3)), the absorption of the beam by the Rb medium is nearly uniform, and both RHP and LHP regions are imaged onto the camera.

Finally, in order to demonstrate the ability to control a spatial polarization all optically, we vary the power of the beam to reduce the absorption of the optical transition (via the effects of optical pumping and saturation), and thus reduce the accompanied dichroism and birefringence. To do so, we use a initial beam of radial polarization, and detune the laser to the regime of dominate CB. In Fig. 4(b,1) and Fig. 4(b,2) we show the Faraday rotation shown before for two distinct power levels (measured before the cell) of 10.8 μW, and 12.6mW (Fig. 4(b,3) & 4(b,4)). As can be seen, a noticeable polarization rotation is observed for the first case, whereas the higher intensity diminishes the polarization rotation effect. Clearly, we are able to control the polarization rotation all optically. Note that all optical control provide flexibility and potentially relatively high switching speed which is directly related to the lifetime of approximately 30ns. The latter can be further enhanced, e.g. by using modified configuration of atomic transitions and the introduction of buffer gas (see e.g [16].).

Here we have applied a slowly varying intensity beam which saturates the atoms in a relatively uniform manner and thus have altered the polarization rotation in a homogeneous fashion. Other exciting possibilities may be the application of spatial dependent beams which will alter the state of polarization spatially, conducting a pump-probe experiment with tightly focused pump beam that will alter the state of polarization locally (and create a defect-like singularity in the polarization), or even using coherent effects such as electromagnetic induced transparency (EIT) to achieve spatial control over the polarization state. may be of great interest as well. Combining the above demonstrated frequency dependent control on the degree of CD & CB together with the possibility to spatial control the polarization all optically may provide a powerful and versatile tool for tailoring the spatial state of polarization.

#256044 Received 18 Dec 2015; revised 13 Feb 2016; accepted 14 Feb 2016; published 25 Feb 2016

4. Summary and conclusions

In summary, we have studied the interaction of space variant polarization beams with Rb in the presence of DC magnetic field, in the linear and non-linear regime. First, we calculated the spatial polarization distribution of three types of space- variant polarization beams: Radially polarized beam, HPB with m = 1; and HPB with m = 2 after being transmitted through atomic vapor having frequency dependent CB and CD. The results show that significant control over the space variant state of polarization can be achieved by controlling the interplay between CD and CB, e.g. via controlling the strength of magnetic field, and wavelength. The obtained effects can be further enhanced, e.g. by controlling the optical density, via temperature control. Furthermore, we verified our findings by measuring the spatial polarization distribution of a radial beam and HPB with m = 1 passing through a Zeeman-shifted Rb medium. The growing interest in the nature and the applications of radially polarized beams brings about the need for new generations of space-variant customized optical tools, one of which is a radial optical isolator. The Faraday effect is the main physical mechanism needed for creating an optical isolator, and implementing the Faraday effect on radially polarized beams is the first step towards creating a radial optical isolator. Furthermore, we have demonstrated that such an apparatus can be used in rapid single shot measurements of polarization rotation, which may serve as an advantage in important applications such as magnetometry. Interestingly, In addition to the ability to control the spatial state of polarization, we have demonstrated the use of the Rb medium as a tunable analyzer for space variant polarization beams. Finally, we have demonstrated the ability to control the CD & CB all optically, by varying the power level launched into the atomic cell, and thus saturating the atomic media.

Our results indicate that the interaction of hot vapors with space variant polarized beams provides additional degrees of freedom in controlling and manipulating the properties of both the beam and the atomic media. The versatility and maturity of the Rb medium, which can be controlled all optically and by static electric and magnetic fields, makes such a combination highly attractive. Specifically, the ability to manipulate the CD and CB all optically, combined with the flexibility of beams with spatially varying polarization paves the way to tailored “pixel-level” polarization control, and thus provides an versatile and powerful tool for manipulating space variant polarized beams.

#256044 Received 18 Dec 2015; revised 13 Feb 2016; accepted 14 Feb 2016; published 25 Feb 2016